Handling of Constraints in Finite-Element Response Sensitivity Analysis

Quan Gu[1]; Michele Barbato[2]; and Joel P. Conte[3]

Abstract: In this paper, the direct differentiation method (DDM) for finite-element (FE) response sensitivity analysis is extended to linear and nonlinear FE models with multi-point constraints (MPCs). The analytical developments are provided for three different constraint handling methods, namely: (1) the transformation equation method; (2) the Lagrange multiplier method; and (3) the penalty function method. Two nonlinear benchmark applications are presented: (1) a two-dimensional soil-foundation-structure interaction system and (2) a three-dimensional, one-bay by one-bay, three-story reinforced concrete building with floor slabs modeled as rigid diaphragms, both subjected to seismic excitation. Time histories of response parameters and their sensitivities to material constitutive parameters are computed and discussed, with emphasis on the relative importance of these parameters in affecting the structural response. The DDM-based response sensitivity results are compared with corresponding forward finite difference analysis results, thus validating the formulation presented and its computer implementation. The developments presented in this paper close an important gap between FE response-only analysis and FE response sensitivity analysis through the DDM, extending the latter to applications requiring response sensitivities of FE models with MPCs. These applications include structural optimization, structural reliability analysis, and finite-element model updating.

DOI: 10.1061/(ASCE)EM.1943-7889.0000053

CE Database subject headings: Finite element method; Constitutive models; Constraints; Sensitivity analysis; Soil-structure interactions.

Introduction

Nonlinear finite-element (FE) analysis is widely recognized as an essential tool in structural analysis and design. In mechanical engineering, computer simulations using complex nonlinear FE models are commonly used in industry during the design process, reducing dramatically the need for prototype tests. In civil engineering, the use of high-fidelity nonlinear models to accurately predict the response of a structural system is even more crucial, due to the fact that prototype testing is not an option. Design codes are gradually accounting for the response of structures well beyond their linear behavior [Advanced Technology Council (ATC-55) 2005]. The state-of-the-art in computational simulation of the static and dynamic response of structural and/or geotechnical systems lies in the nonlinear domain to account for material and geometric nonlinearities governing the complex behavior of such systems, especially near their failure range.

Recent years have seen a growing interest in the analysis of structural response sensitivity to various geometric, mechanical, material, and loading parameters defining a structure and its loading environment. FE response sensitivities represent an essential ingredient for gradient-based optimization methods needed in various sub-fields of structural engineering such as structural optimization, structural reliability analysis, structural identification, and finite-element model updating (Ditlevsen and Madsen 1996; Kleiber et al. 1997; Franchin 2004). In addition, stand-alone FE response sensitivity analysis is invaluable for gaining deeper insight into the effect and relative importance of system and loading parameters in regards to structural response behavior.

FE response sensitivity analysis can be performed accurately and efficiently using the direct differentiation method (DDM), at the one-time cost of deriving and implementing response sensitivity computation algorithms consistently with the algorithms used for response-only computation (Zhang and Der Kiureghian 1993; Conte 2001; Conte et al. 2003). FE response sensitivity analysis capabilities need to be continuously enhanced to take advantage of the state-of-the-art in computational simulation. Indeed, this process is undergoing as shown by the active research in this field in recent years (Conte et al. 2004; Zona et al. 2004; Scott et al. 2004; Barbato and Conte 2005; Haukaas and Der Kiureghian 2005; Zona et al. 2005, 2006; Barbato and Conte 2006; Haukaas and Scott 2006; Barbato et al. 2007; Haukaas and Der Kiureghian 2007; Scott and Filippou 2007; Scott and Haukaas 2008).

This paper extends the use of DDM-based FE response sensitivity analysis to FE models with multi-point constraints (MPCs). MPCs enforce relations among the degrees of freedom (DOFs) at two or more distinct nodes in a FE model (Felippa 2001; Cook et al. 2002). The use of MPCs arises very often in FE structural analysis, e.g., to enforce (1) an equal-displacement behavior (i.e.,

[1]Geotechnical Engineer, AMEC Geomatrix, 510 Superior Ave., Suite 200, Newport Beach, CA 92663. E-mail: qgu@ucsd.edu

[2]Assistant Professor, Dept. of Civil and Environmental Engineering, Louisiana State Univ., 3531 Patrick F. Taylor Hall, Nicholson Extension, Baton Rouge, LA 70803. E-mail: mbarbato@lsu.edu

[3]Professor, Dept. of Structural Engineering, Univ. of California at San Diego, 9500 Gilman Dr., La Jolla, CA 92093-0085 (corresponding author). E-mail: jpconte@ucsd.edu

Note. This manuscript was submitted on September 3, 2008; approved on April 21, 2009; published online on April 24, 2009. Discussion period open until May 1, 2010; separate discussions must be submitted for individual papers. This paper is part of the ***Journal of Engineering Mechanics***, Vol. 135, No. 12, December 1, 2009. ©ASCE, ISSN 0733-9399/2009/12-1427–1438/$25.00.

translations and/or rotations at different nodes are constrained to be equal); (2) a rigid body behavior (i.e., displacements at different nodes are related as if connected with rigid links, e.g., rigid body constraint, rigid diaphragm constraint, rigid plate constraint, rigid rod constraint, and rigid beam constraint); and (3) symmetry and antisymmetry conditions. Therefore, widely used commercial FE programs (e.g., SAP2000, ADINA, and ABAQUS) have rich libraries of MPCs based on several different methods for handling constraints.

Up to date and to the best of the writers' knowledge, a clear analytical and algorithmic treatment of MPCs is missing in the context of DDM-based response sensitivity analysis. The problem has been usually circumvented by using ad hoc modeling solutions (e.g., enforcing approximately MPCs by using very stiff fictitious elements), leading to inefficiency and/or inaccuracy that hampered the advantages of using the DDM. This paper presents a rigorous solution to the problem of handling MPCs in DDM-based FE response sensitivity analysis, thus extending the use of the latter to a broader range of FE models.

Finite-Element Response and Response Sensitivity Analysis

The computation via DDM of FE response sensitivities to material, geometric and loading parameters requires the extension of the FE algorithms for response-only computation. If r denotes a generic scalar response quantity, the sensitivity of r with respect to the material or loading parameter θ is defined as the (absolute) partial derivative of r with respect to θ evaluated at $\theta=\theta_0$, i.e., $\partial r/\partial\theta|_{\theta=\theta_0}$, where θ_0=nominal value of parameter θ.

In the sequel, following the notation proposed by Kleiber et al. (1997), and considering the case of a single sensitivity parameter without loss of generality, the basic equations for FE response and response sensitivity computation are presented following the derivations in Zhang and Der Kiureghian (1993). It is assumed herein that the response of a structural/geotechnical system is computed using a general-purpose nonlinear FE analysis program based on the direct stiffness method, employing suitable numerical integration schemes. After spatial discretization using the FE method, the equations of motion of the considered system can be expressed as

$$\mathbf{M}(\theta)\ddot{\mathbf{u}}(t,\theta)+\mathbf{C}(\theta)\dot{\mathbf{u}}(t,\theta)+\mathbf{R}[\mathbf{u}(t,\theta),\theta]=\mathbf{F}(t,\theta) \tag{1}$$

where t=time; θ=scalar sensitivity parameter considered here as a material constitutive parameter or a loading parameter; $\mathbf{u}$ =vector of nodal displacements; $\mathbf{M}$=mass matrix; $\mathbf{C}$=damping matrix; $\mathbf{R}$=history dependent internal (inelastic) resisting force vector; and $\mathbf{F}$=applied dynamic load vector, and a superposed dot denotes one differentiation with respect to time. In the case of "rigid-soil" earthquake ground excitation, the dynamic load vector takes the form $\mathbf{F}(t,\theta)=-\mathbf{M}(\theta)\mathbf{L}\ddot{u}_g(t,\theta)$ in which $\mathbf{L}$ is an influence coefficient vector and $\ddot{u}_g(t,\theta)$ denotes the input ground acceleration history.

It is assumed that the time continuous—spatially discrete equation of motion (1) is integrated numerically in time using the following general one-step integration algorithm, which contains the Newmark-β and Wilson-θ methods as special cases (see Chopra 2001)

$$\ddot{\mathbf{u}}_{n+1}(\theta)=a_1\mathbf{u}_{n+1}(\theta)+a_2\mathbf{u}_n(\theta)+a_3\dot{\mathbf{u}}_n(\theta)+a_4\ddot{\mathbf{u}}_n(\theta) \tag{2}$$

$$\dot{\mathbf{u}}_{n+1}(\theta)=a_5\mathbf{u}_{n+1}(\theta)+a_6\mathbf{u}_n(\theta)+a_7\dot{\mathbf{u}}_n(\theta)+a_8\ddot{\mathbf{u}}_n(\theta) \tag{3}$$

where a_i $(i=1,\ldots,8)$ are user defined parameters that depend on the specific time-step integration method employed and the subscript $(\ldots)_{n+1}$ indicates that the quantity to which it is attached is evaluated at discrete time t_{n+1}. Substituting Eqs. (2) and (3) in Eq. (1) written at time t_{n+1} yields the following nonlinear matrix algebraic equation in the unknowns $\mathbf{u}_{n+1}=\mathbf{u}(t_{n+1})$ to be solved at each time step $[t_n,t_{n+1}]$:

$$\{a_1\mathbf{M}(\theta)\mathbf{u}_{n+1}(\theta)+a_5\mathbf{C}(\theta)\mathbf{u}_{n+1}(\theta)+\mathbf{R}[\mathbf{u}_{n+1}(\theta),\theta]\}-\tilde{\mathbf{F}}_{n+1}(\theta)=\mathbf{0} \tag{4}$$

where

$$\tilde{\mathbf{F}}_{n+1}(\theta)=\mathbf{F}_{n+1}(\theta)-\mathbf{M}(\theta)[a_2\mathbf{u}_n(\theta)+a_3\dot{\mathbf{u}}_n(\theta)+a_4\ddot{\mathbf{u}}_n(\theta)]-\mathbf{C}(\theta)[a_6\mathbf{u}_n(\theta)+a_7\dot{\mathbf{u}}_n(\theta)+a_8\ddot{\mathbf{u}}_n(\theta)] \tag{5}$$

Assuming that $\mathbf{u}_{n+1}$ is the converged solution (up to some iteration residuals) for the current time step $[t_n,t_{n+1}]$, and differentiating analytically Eq. (4) with respect to θ yields the response sensitivity equation at the structure level

$$\mathbf{K}_{n+1}^{\text{dyn}}(\theta)\cdot\frac{d\mathbf{u}_{n+1}}{d\theta}=\left(\frac{d\mathbf{F}}{d\theta}\right)_{n+1}^{\text{dyn}}-\left.\frac{\partial\mathbf{R}[\mathbf{u}_{n+1}(\theta),\theta]}{\partial\theta}\right|_{\mathbf{u}_{n+1}} \tag{6}$$

where

$$\left(\frac{d\mathbf{F}}{d\theta}\right)_{n+1}^{\text{dyn}}=\frac{d\tilde{\mathbf{F}}_{n+1}}{d\theta}-\left(a_1\frac{d\mathbf{M}}{d\theta}+a_5\frac{d\mathbf{C}}{d\theta}\right)\mathbf{u}_{n+1}(\theta) \tag{7}$$

$$\mathbf{K}_{n+1}^{\text{dyn}}(\theta)=a_1\mathbf{M}(\theta)+a_5\mathbf{C}(\theta)+\mathbf{K}_{n+1}(\theta) \tag{8}$$

where $\mathbf{K}_{n+1}$=static consistent tangent stiffness matrix of the structure at time t_{n+1}.

The above formulation, derived explicitly for dynamic response sensitivity analysis, contains the quasi-static case as a particular case, obtained simply by discarding in Eqs. (4)–(8) all terms involving the mass and damping matrices as well as their derivatives with respect to the sensitivity parameter θ. In particular, the equilibrium equations, Eq. (4), and the sensitivity equations, Eq. (6), reduce to

$$\mathbf{R}[\mathbf{u}_{n+1}(\theta),\theta]-\mathbf{F}_{n+1}(\theta)=\mathbf{0} \tag{9}$$

$$\mathbf{K}_{n+1}(\theta)\cdot\frac{d\mathbf{u}_{n+1}}{d\theta}=\frac{d\mathbf{F}_{n+1}}{d\theta}-\left.\frac{\partial\mathbf{R}[\mathbf{u}_{n+1}(\theta),\theta]}{\partial\theta}\right|_{\mathbf{u}_{n+1}} \tag{10}$$

Handling of Constraints

Response Computation

Constraints enforce additional conditions on the DOFs of a given FE model. More specifically, a constraint either prescribes the value of a DOF ("single-point constraint" or "single freedom constraint," e.g., support conditions) or prescribes a relation among two or more DOFs ("MPC" or "multifreedom constraint," e.g., rigid links, rigid elements, and rigid diaphragms) (Felippa 2001; Cook et al. 2002). Furthermore, MPCs can be differentiated in "linear" and "nonlinear" constraints, i.e., they can prescribe linear or nonlinear relations among DOFs. In FE analysis of structural systems, linear constraints are very common.

Handling of single-point constraints is an easy task and reduces to eliminating the constrained DOFs from the equations of motion (dynamic case) or the equations of equilibrium (quasi-static case). Handling of MPCs requires introducing a set of equations that couple the DOFs affected by the constraints, called "constraint equations." For linear MPCs, the constraint equations can be expressed in the following matrix form

$$\mathbf{A}\mathbf{u}_{n+1}(\theta) = \mathbf{Q} \tag{11}$$

where $\mathbf{A}$=constant matrix and $\mathbf{Q}$=constant vector. In general, matrix $\mathbf{A}$ and vector $\mathbf{Q}$ may depend on some (e.g., geometric) parameters that are not considered as sensitivity parameters in this paper.

Three different methods are available in the literature for imposing MPCs, namely: (1) the "transformation equation method" or "master-slave elimination"; (2) the "Lagrange multiplier method" or "Lagrange multiplier adjunction"; and (3) the "penalty function method" or "penalty augmentation." These three methods are well known and widely applied for response-only computation (Felippa 2001; Cook et al. 2002). Herein, the basic ideas underlying these methods are recalled for response-only computation, while the full DDM-based response sensitivity algorithm is developed and presented in the following section for each of these three constraint handling methods. It is noteworthy that any type of linear MPCs (e.g., equal DOF, rigid link, and rigid diaphragm) can be handled using the three different methods considered in this paper.

The transformation equation method requires to partition the equations of motion (equilibrium) and the constraint equations between retained (or master) DOFs (denoted by the subscript "r") and DOFs to be eliminated or condensed out (denoted by the subscript "c" and also called slave DOFs). After some algebraic manipulations, the slave DOFs are explicitly eliminated and the equations of motion (equilibrium) at the structure level are expressed only in terms of the retained DOFs. The number of equations of static/dynamic equilibrium to be solved is reduced by one for each constraint equation introduced.

The Lagrange multiplier method requires the introduction of additional variables $\boldsymbol{\lambda}$ (Lagrange multipliers). The constraints are replaced by a system of applied nodal forces called constraint forces, which enforce the constraints. Nodal displacements and Lagrange multipliers are computed simultaneously, thus augmenting the number of equations to be solved by one for each constraint.

The penalty function method introduces in the equations of motion (equilibrium) some penalty terms which can be physically interpreted as fictitious high stiffness elastic elements enforcing the constraint approximately. Each of these fictitious elements is parameterized by a numerical weight ("penalty weight" or "penalty number"), such that the constraint is satisfied exactly if the weight goes to infinity. The problem size (i.e., number of equations to be solved) is unchanged, but the constraints are imposed only approximately.

The considered DDM formulation and its extension to account for MPCs can be used for FE models including both material and geometric nonlinearities (Haukaas and Scott 2006; Scott and Filippou 2007; Barbato et al. 2007). The FE response sensitivity algorithms presented in this paper extend the DDM to linear and geometrically/materially nonlinear FE models with linear MPCs, including a comprehensive study of several MPC handling techniques.

Response Sensitivity Computation

The DDM-based FE response sensitivity computation is based on the same set of equations for all three methods considered, i.e.

$$\begin{cases} \{a_1\mathbf{M}(\theta)\mathbf{u}_{n+1}(\theta) + a_5\mathbf{C}(\theta)\mathbf{u}_{n+1}(\theta) + \mathbf{R}[\mathbf{u}_{n+1}(\theta),\theta]\} - \tilde{\mathbf{F}}_{n+1}(\theta) = \mathbf{0} \\ \mathbf{A}\mathbf{u}_{n+1}(\theta) = \mathbf{Q} \\ \mathbf{A}\dot{\mathbf{u}}_{n+1}(\theta) = \mathbf{0} \\ \mathbf{A}\ddot{\mathbf{u}}_{n+1}(\theta) = \mathbf{0} \end{cases} \tag{12}$$

and

$$\begin{cases} \mathbf{R}[\mathbf{u}_{n+1}(\theta),\theta] - \mathbf{F}_{n+1}(\theta) = \mathbf{0} & (13a) \\ \mathbf{A}\mathbf{u}_{n+1}(\theta) = \mathbf{Q} & (13b) \end{cases}$$

for the dynamic and quasi-static analysis case, respectively. In the sequel: (1) the subscript "$n+1$" is dropped; (2) the derivations are explicitly carried out for the quasi-static analysis case; and (3) the final governing sensitivity equations are presented for the more general dynamic analysis case without derivations, since these equations can be readily obtained from the quasi-static case.

Transformation Equation Method

The structure nodal displacement vector $\mathbf{u}$, nodal resisting force vector $\mathbf{R}$, nodal applied force vector $\mathbf{F}$, and tangent stiffness matrix $\mathbf{K}$ are partitioned into DOFs to be retained (subscript "r") and DOFs to be condensed out (subscript "c") as

$$\mathbf{u}(\theta) = \begin{bmatrix} \mathbf{u}_r(\theta) \\ \mathbf{u}_c(\theta) \end{bmatrix} \tag{14a}$$

$$\mathbf{R}(\theta) = \begin{bmatrix} \mathbf{R}_r(\theta) \\ \mathbf{R}_c(\theta) \end{bmatrix} \tag{14b}$$

$$\mathbf{F}(\theta) = \begin{bmatrix} \mathbf{F}_r(\theta) \\ \mathbf{F}_c(\theta) \end{bmatrix} \tag{14c}$$

$$\mathbf{K}(\theta) = \begin{bmatrix} \mathbf{K}_{rr}(\theta) & \mathbf{K}_{rc}(\theta) \\ \mathbf{K}_{cr}(\theta) & \mathbf{K}_{cc}(\theta) \end{bmatrix} \tag{14d}$$

Partitioning also the constraint matrix $\mathbf{A}$ as $\mathbf{A}=[\mathbf{T}_r\mathbf{T}_c]$, Eq. (13) can be rewritten as

$$\begin{cases} \mathbf{R}_e[\mathbf{u}_\mathbf{r}(\theta),\theta] - \mathbf{F}_e(\theta) = \mathbf{0} & (15a) \\ \mathbf{u}_c(\theta) = \mathbf{T}_{rc}\mathbf{u}_\mathbf{r}(\theta) + \mathbf{T}_c^{-1}\mathbf{Q} & (15b) \end{cases}$$

where

$$\begin{cases} \mathbf{R}_e(\theta) = \mathbf{R}_r(\theta) + \mathbf{T}_{rc}^T\mathbf{R}_c(\theta) & (16a) \\ \mathbf{F}_e(\theta) = \mathbf{F}_r(\theta) + \mathbf{T}_{rc}^T\mathbf{F}_c(\theta) & (16b) \end{cases}$$

and $\mathbf{T}_{rc}=-\mathbf{T}_c^{-1}\mathbf{T}_r$ in which the inverse of matrix $\mathbf{T}_c$ exists if the imposed MPCs are linearly independent. The subscript "e" denotes equivalent (or condensed) quantities. The external forces $\mathbf{F}_e$ applied along DOFs $\mathbf{u}_r$ are equivalent (in the sense of equilibrium) to the applied external forces $\mathbf{F}_r$ and $\mathbf{F}_c$ which produce $\mathbf{u}_r$ and $\mathbf{u}_c$ satisfying the constraint equation, Eq. (13b). The relation between the equivalent internal forces $\mathbf{R}_e$ (acting at DOFs $\mathbf{u}_r$) and the internal resisting forces $\mathbf{R}_r$ and $\mathbf{R}_c$ (acting at DOFs $\mathbf{u}_r$ and $\mathbf{u}_c$, respectively) is similar to that between $\mathbf{F}_e$, $\mathbf{F}_r$, and $\mathbf{F}_c$.

Differentiating Eqs. (15b) and (16a) with respect to sensitivity parameter θ yields, respectively

$$\frac{d\mathbf{u}_c}{d\theta} = \mathbf{T}_{rc}\frac{d\mathbf{u}_r}{d\theta} \tag{17}$$

and

$$\frac{d\mathbf{R}_e}{d\theta} = \frac{d\mathbf{R}_r}{d\theta} + \mathbf{T}_{rc}^T\frac{d\mathbf{R}_c}{d\theta} \tag{18}$$

Differentiating $\mathbf{R}_r$ and $\mathbf{R}_c$ with respect to θ, recognizing from Eqs. (9), (14*a*), and (14*b*) that $\mathbf{R}_r = \mathbf{R}_r[\mathbf{u}_r(\theta), \mathbf{u}_c(\theta), \theta]$ and $\mathbf{R}_c = \mathbf{R}_c[\mathbf{u}_r(\theta), \mathbf{u}_c(\theta), \theta]$, using the chain rule of differentiation and the theorem of differentiation of implicit functions yields

$$\begin{cases} \dfrac{d\mathbf{R}_r}{d\theta} = \mathbf{K}_{rr}(\theta)\dfrac{d\mathbf{u}_r}{d\theta} + \mathbf{K}_{rc}(\theta)\dfrac{d\mathbf{u}_c}{d\theta} + \left.\dfrac{\partial \mathbf{R}_r}{\partial \theta}\right|_{\mathbf{u}} \\ \dfrac{d\mathbf{R}_c}{d\theta} = \mathbf{K}_{cr}(\theta)\dfrac{d\mathbf{u}_r}{d\theta} + \mathbf{K}_{cc}(\theta)\dfrac{d\mathbf{u}_c}{d\theta} + \left.\dfrac{\partial \mathbf{R}_c}{\partial \theta}\right|_{\mathbf{u}} \end{cases} \tag{19}$$

in which

$$\mathbf{K}_{rr}(\theta) = \left.\frac{\partial \mathbf{R}_r}{\partial \mathbf{u}_r}\right|_{\theta}, \quad \mathbf{K}_{rc}(\theta) = \left.\frac{\partial \mathbf{R}_r}{\partial \mathbf{u}_c}\right|_{\theta}$$

$$\mathbf{K}_{cr}(\theta) = \left.\frac{\partial \mathbf{R}_c}{\partial \mathbf{u}_r}\right|_{\theta}, \text{ and } \mathbf{K}_{cc}(\theta) = \left.\frac{\partial \mathbf{R}_c}{\partial \mathbf{u}_c}\right|_{\theta}$$

Substituting Eq. (17) into Eq. (19) and the resulting equation into Eq. (18) yields

$$\frac{d\mathbf{R}_e}{d\theta} = [\mathbf{K}_{rr}(\theta) + \mathbf{K}_{rc}(\theta)\mathbf{T}_{rc} + \mathbf{T}_{rc}^T\mathbf{K}_{cr}(\theta) + \mathbf{T}_{rc}^T\mathbf{K}_{cc}(\theta)\mathbf{T}_{rc}]\frac{d\mathbf{u}_r}{d\theta} + \left(\left.\frac{\partial \mathbf{R}_r}{\partial \theta}\right|_{\mathbf{u}} + \mathbf{T}_{rc}^T \left.\frac{\partial \mathbf{R}_c}{\partial \theta}\right|_{\mathbf{u}} \right) \tag{20}$$

Finally, differentiating Eq. (15*a*) with respect to θ and substituting Eq. (20) in the resulting equation yields the following sensitivity equations for quasi-static analysis

$$\begin{cases} \mathbf{K}_e(\theta)\cdot\dfrac{d\mathbf{u}_r}{d\theta} = \dfrac{d\mathbf{F}_e}{d\theta} - \left.\dfrac{\partial \mathbf{R}_e}{\partial \theta}\right|_{\mathbf{u}} \\ \dfrac{d\mathbf{u}_c}{d\theta} = \mathbf{T}_{rc}\dfrac{d\mathbf{u}_r}{d\theta} \end{cases} \tag{21}$$

where

$$\mathbf{K}_e(\theta) = \left.\frac{\partial \mathbf{R}_e}{\partial \mathbf{u}_r}\right|_{\theta} = \mathbf{K}_{rr}(\theta) + \mathbf{K}_{rc}(\theta)\mathbf{T}_{rc} + \mathbf{T}_{rc}^T\mathbf{K}_{cr}(\theta) + \mathbf{T}_{rc}^T\mathbf{K}_{cc}(\theta)\mathbf{T}_{rc} \tag{22}$$

$$\left.\frac{\partial \mathbf{R}_e}{\partial \theta}\right|_{\mathbf{u}} = \left.\frac{\partial \mathbf{R}_r}{\partial \theta}\right|_{\mathbf{u}} + \mathbf{T}_{rc}^T \left.\frac{\partial \mathbf{R}_c}{\partial \theta}\right|_{\mathbf{u}} \tag{23}$$

It is worth to point out that prior to computing response sensitivities at each load/time step, the equivalent tangent stiffness matrix $\mathbf{K}_e$ in Eq. (21) has already been computed and factorized for calculating the response. Thus, solution of Eq. (21) is computationally efficient.

Following a similar derivation as in Eqs. (17)–(23), the sensitivity equations for dynamic analysis are given by (recalling that the subscript "$n+1$" has been dropped)

$$\begin{cases} \mathbf{K}_e^{\text{dyn}}(\theta)\cdot\dfrac{d\mathbf{u}_r}{d\theta} = \left(\dfrac{d\mathbf{F}}{d\theta}\right)_e^{\text{dyn}} - \left.\dfrac{\partial \mathbf{R}_e}{\partial \theta}\right|_{\mathbf{u}} \\ \dfrac{d\mathbf{u}_c}{d\theta} = \mathbf{T}_{rc}\dfrac{d\mathbf{u}_r}{d\theta} \\ \dfrac{d\ddot{\mathbf{u}}}{d\theta} = a_1\dfrac{d\mathbf{u}}{d\theta} + a_2\dfrac{d\mathbf{u}_n}{d\theta} + a_3\dfrac{d\dot{\mathbf{u}}_n}{d\theta} + a_4\dfrac{d\ddot{\mathbf{u}}_n}{d\theta} \\ \dfrac{d\dot{\mathbf{u}}}{d\theta} = a_5\dfrac{d\mathbf{u}}{d\theta} + a_6\dfrac{d\mathbf{u}_n}{d\theta} + a_7\dfrac{d\dot{\mathbf{u}}_n}{d\theta} + a_8\dfrac{d\ddot{\mathbf{u}}_n}{d\theta} \end{cases} \tag{24}$$

where

$$\mathbf{K}_e^{\text{dyn}}(\theta) = a_1\mathbf{M}_e(\theta) + a_5\mathbf{C}_e(\theta) + \mathbf{K}_e(\theta) \tag{25}$$

$$\left(\frac{d\mathbf{F}}{d\theta}\right)_e^{\text{dyn}} = \frac{d\tilde{\mathbf{F}}_e}{d\theta} - \left(a_1\frac{d\mathbf{M}_e}{d\theta} + a_5\frac{d\mathbf{C}_e}{d\theta}\right)\mathbf{u}_r(\theta) \tag{26}$$

In Eqs. (24)–(26), the following matrix partitioning and definition of equivalent matrix are employed

$$\boldsymbol{M} = \begin{bmatrix} \boldsymbol{M}_{rr} & \boldsymbol{M}_{rc} \\ \boldsymbol{M}_{cr} & \boldsymbol{M}_{cc} \end{bmatrix} \quad \text{and}$$

$$\boldsymbol{M}_e = \boldsymbol{M}_{rr} + \boldsymbol{M}_{rc}\mathbf{T}_{rc} + \mathbf{T}_{rc}^T\boldsymbol{M}_{cr} + \mathbf{T}_{rc}^T\boldsymbol{M}_{cc}\mathbf{T}_{rc} \tag{27}$$

in which the matrix quantities considered are $\boldsymbol{M} = \mathbf{M}, \mathbf{C}, d\mathbf{M}/d\theta, d\mathbf{C}/d\theta$. Similarly, the following vector partitioning and definition of equivalent vector are also used:

$$\boldsymbol{V} = \begin{bmatrix} \boldsymbol{V}_r \\ \boldsymbol{V}_c \end{bmatrix} \quad \text{and} \quad \boldsymbol{V}_e = \boldsymbol{V}_r + \mathbf{T}_{rc}^T\boldsymbol{V}_c \tag{28}$$

in which the vector quantities considered are $\boldsymbol{V} = d\tilde{\mathbf{F}}/d\theta$, $(d\mathbf{F}/d\theta)^{\text{dyn}}$.

It is important to recognize that correct application of the DDM requires the updating of the complete (retained and condensed out DOFs) vectors of nodal displacement, velocity and acceleration response sensitivities at each time step.

Lagrange Multiplier Method

Eq. (13) is rewritten as (Felippa 2001)

$$\begin{cases} \mathbf{R}[\mathbf{u}(\theta), \theta] + \mathbf{A}^T\boldsymbol{\lambda}(\theta) - \mathbf{F}(\theta) = \mathbf{0} \\ \mathbf{A}\mathbf{u}(\theta) - \mathbf{Q} = \mathbf{0} \end{cases} \tag{29}$$

where $\boldsymbol{\lambda}$ = vector of Lagrange multipliers. This augmented set of equations needs to be solved simultaneously for all variables (i.e., $\mathbf{u}$ and $\boldsymbol{\lambda}$) in both linear and nonlinear analysis. The number of equations to be solved is equal to the sum of the number of unrestrained (free) DOFs and the number of imposed constraints. In the Lagrange multiplier method, the constraints are replaced by a system of applied nodal forces $-\mathbf{A}^T\boldsymbol{\lambda}$, called constraint forces, which enforce the constraints exactly. Thus, it is clear that the Lagrange multipliers $\boldsymbol{\lambda}$ are functions of the sensitivity parameters considered in this study (i.e., material and loading parameters).

For the purpose of response sensitivity analysis, the governing equilibrium equations for the response, Eq. (29), are differentiated with respect to θ to obtain the following response sensitivity equations (in matrix form) in the case of quasi-static analysis:

$$\begin{bmatrix} \mathbf{K} & \mathbf{A}^T \\ \mathbf{A} & \mathbf{0} \end{bmatrix} \begin{Bmatrix} \frac{d\mathbf{u}}{d\theta} \\ \frac{d\boldsymbol{\lambda}}{d\theta} \end{Bmatrix} = \begin{Bmatrix} \frac{d\mathbf{F}}{d\theta} - \left.\frac{\partial \mathbf{R}}{\partial \theta}\right|_{\mathbf{u}} \\ \mathbf{0} \end{Bmatrix} \tag{30}$$

In the dynamic analysis case, the response sensitivity equations become (recalling that the subscript "$n+1$" has been dropped)

$$\begin{cases} \begin{bmatrix} \mathbf{K}^{\text{dyn}} & \mathbf{A}^T \\ \mathbf{A} & \mathbf{0} \end{bmatrix} \begin{Bmatrix} \frac{d\mathbf{u}}{d\theta} \\ \frac{d\boldsymbol{\lambda}}{d\theta} \end{Bmatrix} = \begin{Bmatrix} \left(\frac{d\mathbf{F}}{d\theta}\right)^{\text{dyn}} - \left.\frac{\partial \mathbf{R}}{\partial \theta}\right|_{\mathbf{u}} \\ \mathbf{0} \end{Bmatrix} \\ \frac{d\ddot{\mathbf{u}}}{d\theta} = a_1 \frac{d\mathbf{u}}{d\theta} + a_2 \frac{d\mathbf{u}_n}{d\theta} + a_3 \frac{d\dot{\mathbf{u}}_n}{d\theta} + a_4 \frac{d\ddot{\mathbf{u}}_n}{d\theta} \\ \frac{d\dot{\mathbf{u}}}{d\theta} = a_5 \frac{d\mathbf{u}}{d\theta} + a_6 \frac{d\mathbf{u}_n}{d\theta} + a_7 \frac{d\dot{\mathbf{u}}_n}{d\theta} + a_8 \frac{d\ddot{\mathbf{u}}_n}{d\theta} \end{cases} \tag{31}$$

Penalty Function Method

The following equation is constructed from Eq. (13) (Felippa 2001)

$$\mathbf{R}[\mathbf{u}(\theta),\theta] + (\mathbf{A}^T\boldsymbol{\alpha}\mathbf{A})\mathbf{u}(\theta) - \mathbf{F}(\theta) - \mathbf{A}^T\boldsymbol{\alpha}\mathbf{Q} = \mathbf{0} \tag{32}$$

where $\boldsymbol{\alpha}$=diagonal matrix of penalty weights, with $\alpha_{ii}>0$ and $\alpha_{ij}=0$ for $i \neq j$ ($i,j=1,2,\ldots,n_{\text{DOF}}$ in which n_{DOF}=number of unrestrained DOFs). For conservative systems, Eq. (32) is obtained from minimization of the potential energy of the considered structural system augmented by the penalty function $1/2(\mathbf{Au}-\mathbf{Q})^T\boldsymbol{\alpha}(\mathbf{Au}-\mathbf{Q})$, also called Courant quadratic penalty function (see Felippa 2001), i.e., equating to zero the derivative of the augmented potential energy with respect to $\mathbf{u}$. The penalty terms introduced in the governing equilibrium equations, Eq. (32), can be physically interpreted as forces acting in fictitious high stiffness elastic elements enforcing the constraint approximately. The term $\mathbf{A}^T\boldsymbol{\alpha}\mathbf{A}$ is commonly referred to as "penalty matrix." The stiffnesses of these fictitious elements are parameterized by the penalty weights α_{ii} so that the constraints are satisfied exactly if these weights go to infinity, in which case the solutions of Eqs. (13) and (32) coincide. In the case of structural systems with nonlinear hysteretic material behavior (i.e., nonconservative systems), Eq. (32) is obtained through the introduction of the penalty terms by analogy with conservative systems.

The number of equations to be solved in Eq. (32) is the same as for the unconstrained structural system, but the constraints are imposed only approximately for finite values of the penalty weights α_{ii}. Particular care is needed in the choice of the penalty weights to balance the trade-off between reducing the constraint violation, which requires to increase the penalty weights, and limiting the solution error due to ill-conditioning with respect to inversion of the modified tangent stiffness matrix, $\mathbf{K}+(\mathbf{A}^T\boldsymbol{\alpha}\mathbf{A})$, at a given iteration of a given load step. This ill-conditioning increases for increasing values of the penalty weights.

For response sensitivity analysis, the governing equilibrium equations in Eq. (32) are differentiated with respect to θ yielding the following response sensitivity equations for quasi-static analysis:

$$[\mathbf{K}+(\mathbf{A}^T\boldsymbol{\alpha}\mathbf{A})]\cdot\frac{d\mathbf{u}}{d\theta} = \frac{d\mathbf{F}}{d\theta} - \left.\frac{\partial \mathbf{R}}{\partial \theta}\right|_{\mathbf{u}} \tag{33}$$

In the dynamic analysis case, the response sensitivity equations are given by (recalling that the subscript "$n+1$" has been dropped)

$$\begin{cases} [\mathbf{K}^{\text{dyn}}+(\mathbf{A}^T\boldsymbol{\alpha}\mathbf{A})]\cdot\frac{d\mathbf{u}}{d\theta} = \left(\frac{d\mathbf{F}}{d\theta}\right)^{\text{dyn}} - \left.\frac{\partial \mathbf{R}}{\partial \theta}\right|_{\mathbf{u}} \\ \frac{d\ddot{\mathbf{u}}}{d\theta} = a_1 \frac{d\mathbf{u}}{d\theta} + a_2 \frac{d\mathbf{u}_n}{d\theta} + a_3 \frac{d\dot{\mathbf{u}}_n}{d\theta} + a_4 \frac{d\ddot{\mathbf{u}}_n}{d\theta} \\ \frac{d\dot{\mathbf{u}}}{d\theta} = a_5 \frac{d\mathbf{u}}{d\theta} + a_6 \frac{d\mathbf{u}_n}{d\theta} + a_7 \frac{d\dot{\mathbf{u}}_n}{d\theta} + a_8 \frac{d\ddot{\mathbf{u}}_n}{d\theta} \end{cases} \tag{34}$$

In order to obtain consistent response sensitivities (Conte et al. 2003), the penalty weights in the sensitivity equations, Eqs. (33) and (34) must be equal to the penalty weights used for response computation in Eq. (32). Clearly, the choice of the penalty weight values affects the accuracy of both response and response sensitivity, but in a consistent way.

Validation Examples

The DDM-based response sensitivity computation algorithms for handling MPCs presented above were implemented by the writers in the finite-element analysis software framework OpenSees (Mazzoni et al. 2005; Gu 2008). OpenSees is an open source object-oriented software framework written in C++ programming language for static and dynamic, linear and nonlinear FE analysis of structural and/or geotechnical systems. OpenSees provides capabilities for response, response sensitivity and reliability analyses of structural, geotechnical and soil-foundation-structure interaction (SFSI) systems. Algorithms for response-only analysis based on FE models with MPCs were already implemented in OpenSees for all three constraint handling methods considered in this paper. Extension of these algorithms to enable response sensitivity analysis while using FE models with MPCs greatly enhances the existing capabilities of OpenSees. To date, the MPCs available in OpenSees are: (1) "equal DOF," which enforces equal displacements/rotations at different DOFs of the FE model; (2) "rigid link," which imposes a rigid connection between different DOFs; and (3) "rigid diaphragm," which imposes a rigid behavior for the in-plane motion of nodes belonging to the same plane.

The methodology presented in this paper for DDM-based FE response sensitivity computation and its software implementation was validated by comparing DDM and forward finite difference (FFD) analysis results for several application examples using all three constraint handling methods considered. Due to space limitation, only selected results from two benchmark applications analyzed using the transformation equation method are presented in the following sections. It is noteworthy that, for each application example considered, FE response and response sensitivity results obtained using different constraint handling methods present only negligible differences, which are related to the convergence tolerance used for response analysis.

Two-Dimensional Soil-Foundation-Structure Interaction System

The first application example consists of a two-dimensional SFSI system subjected to earthquake excitation. The structure is a two-

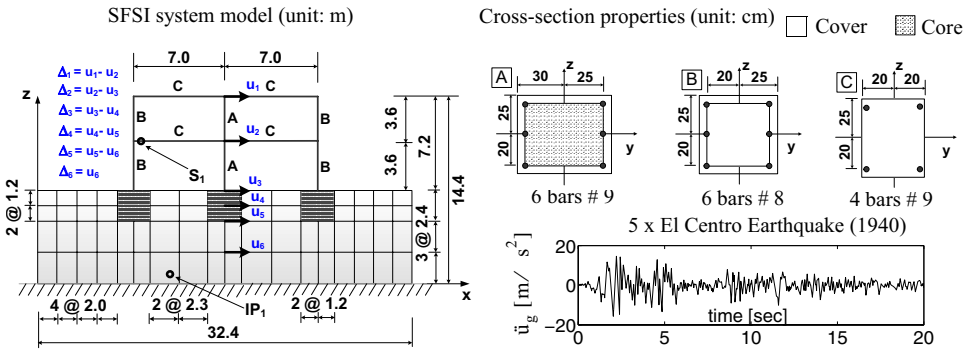

Fig. 1. 2D model of SFSI system: geometry, cross-sectional properties of structural members, and input ground motion

story, two-bay, reinforced concrete frame, as shown in Fig. 1. The foundations consist of reinforced concrete square footings below each column. The foundation soil is a layered clay with material properties varying along the depth.

The frame structure of this SFSI system is modeled by using displacement-based Euler-Bernoulli frame elements with distributed plasticity and four Gauss-Legendre integration points. Every physical beam and column is discretized into three and two frame elements, respectively, of equal length. Section stress resultants at the integration points are computed by using fiber sections with concrete and reinforcing steel material layers. The concrete material is modeled using the Kent-Scott-Park model with no tension stiffening (Scott et al. 1982). The concrete constitutive parameters are: f_c=concrete peak strength in compression; f_u=residual strength; ε_0=strain at peak strength; and ε_u=strain at which the residual strength is reached. Different material parameters are used for the confined (identified by the subscript "core") and unconfined (identified by the subscript "cover") concrete in the columns. The constitutive behavior of the reinforcing steel is modeled using the one-dimensional J_2 plasticity model with linear kinematic and isotropic hardening (Conte et al. 2003). The material parameters defining the J_2 plasticity model are: E=Young's modulus; f_y=yield strength; H_{kin}=kinematic hardening modulus; and H_{iso}=isotropic hardening modulus.

The foundation footings and soil layers are modeled using isoparametric four-node quadrilateral finite elements with bilinear displacement interpolation. The foundation footings are modeled as linear elastic with Young's modulus $E=20,000$ MPa and Poisson's ratio $\nu=0.20$. The soil mesh is shown in Fig. 1. The soil domain is assumed to be under plane strain condition with a constant soil thickness of 4 m, corresponding to the interframe distance. The soil materials are modeled using a pressure-independent multi-yield-surface J_2 plasticity model (Prevost 1977; Q. Gu et al. 2009) specialized for plane strain condition. Each of the four soil layers is characterized by a different set of material parameters, namely, G_i=low strain shear modulus, B_i=bulk modulus, τ_i=shear strength, with $i=1,2,3,4$ corresponding to the numbering of the soil layers (from top to bottom).

The three types of material constitutive models used in this application example are shown in Fig. 2, together with the values of the constitutive parameters. The inertia properties of the frame structure are modeled through translational masses lumped at the nodes, taking into account the structure own weight, as well as dead and live loads. The inertia properties of the soil mesh are represented through lumped element mass matrices computed from the soil mass density taken as $2,000$ kg/m^3 for all soil layers.

A crucial point in modeling SFSI systems such as the one considered here is the use of MPCs in order to: (1) enforce displacement compatibility at the interface between structural (frame) elements and continuum (quadrilateral) elements (column-footing connections), and (2) impose a simple shear condition for the soil (see Fig. 3). These modeling requirements are satisfied by using the equal DOF type of MPC.

FE response and response sensitivity analyses are performed using the model described above. After quasi-static application of the gravity loads (modeled as vertical forces concentrated at the nodes of the FE mesh), earthquake excitation is applied by imposing a total acceleration time history at the base of the computational soil domain. The ground acceleration time history considered is the balanced 1940 El Centro earthquake record scaled by a factor of 5 (Fig. 1). Response sensitivities to all material parameters (four parameters for the confined concrete, four for the unconfined concrete, four for the reinforcing steel, three

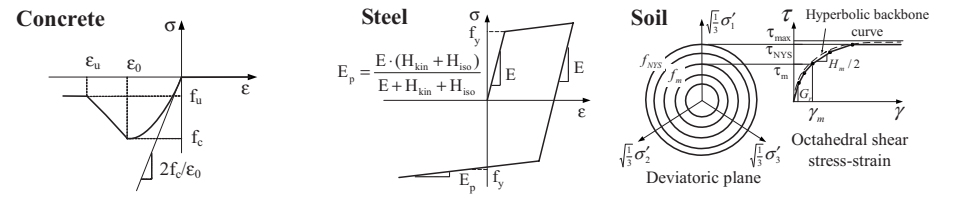

Par.	Confined	Unconfined	Unit
ε_0	0.004	0.002	-
ε_u	0.014	0.008	-
f_c	34.5	27.6	MPa
f_u	20.7	0.0	MPa

Par.	Value
E [MPa]	200000
f_y [MPa]	248.2
H_{kin} [MPa]	1612.9
H_{iso} [MPa]	0

Layer #	G_i [kPa]	B_i [MPa]	τ_i [kPa]
1	54450	160	33
2	33800	100	26
3	61250	180	35
4	96800	290	44

Fig. 2. Material constitutive models used in the SFSI model

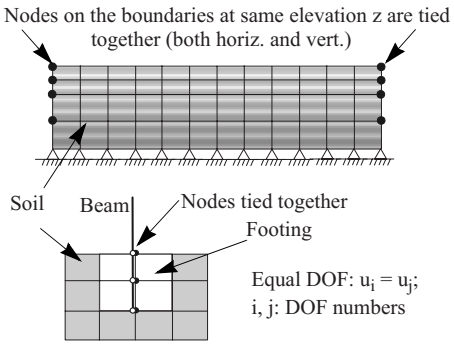

Fig. 3. Multipoint constraints used in the SFSI model: equal DOF

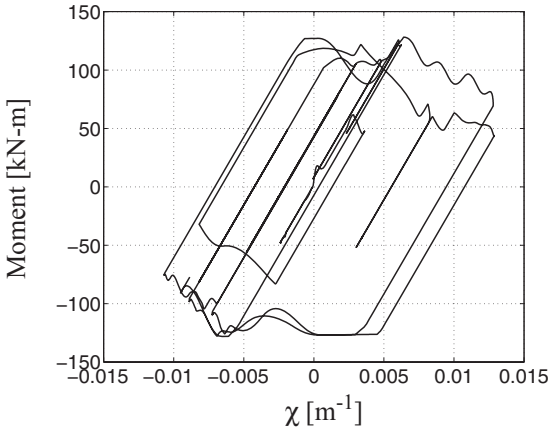

Fig. 6. Response of the 2D SFSI system: moment-curvature hysteretic response at section S_1 (see Fig. 1)

for each of the four soil layers, and two for the elastic foundation footings for a total of 26 material parameters) are computed using the DDM.

Figs. 4 and 5 show the time histories of the interstory drifts (at the middle column) and soil interlayer drifts (at the nodes below the middle column), respectively. In Fig. 4, it is observed that the time histories of the two interstory drifts are very similar, since the overall rotation (rocking) of the structure due to soil flexibility produces a major contribution to the floor horizontal displacements. Fig. 6 displays the moment-curvature hysteretic response at the left-most Gauss-Legendre integration point of the left beam at the first story, identified in Fig. 1 as Section 1 (S_1). Fig. 7 provides the shear stress-strain hysteretic response at Integration Point 1 (IP_1, see Fig. 1) near the bottom of the soil mesh. From Figs. 5–7, it is observed that, during the earthquake considered, the SFSI system undergoes significant inelastic behavior in both the structure and the foundation soil. In particular, large inelastic and residual interlayer drifts are induced in the bottom soil layer (see Fig. 5) due to (1) the high intensity earthquake excitation considered (peak ground acceleration at the base of the computational soil domain=1.59 g) and (2) the low postyield shear stiffness in the clay soil model.

In conjunction with the FE response analysis, a FE response sensitivity analysis is performed. Asymptotic convergence of FFD analysis results (i.e., convergence for increasingly smaller perturbations of the sensitivity parameter) to DDM results has been

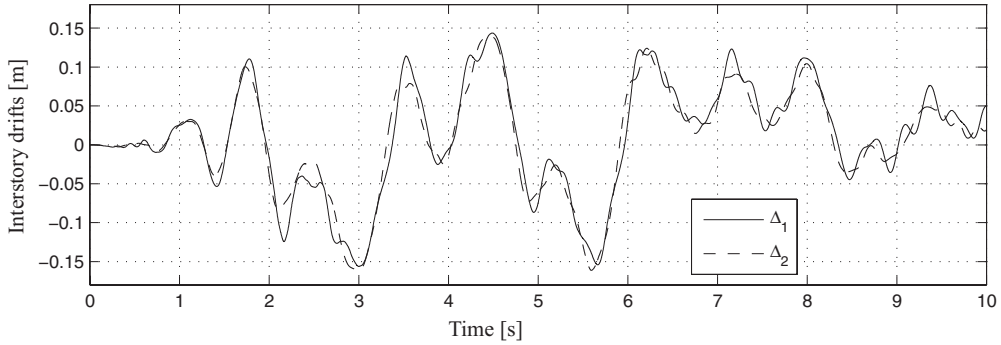

Fig. 4. Response of the 2D SFSI system: time histories of interstory drifts

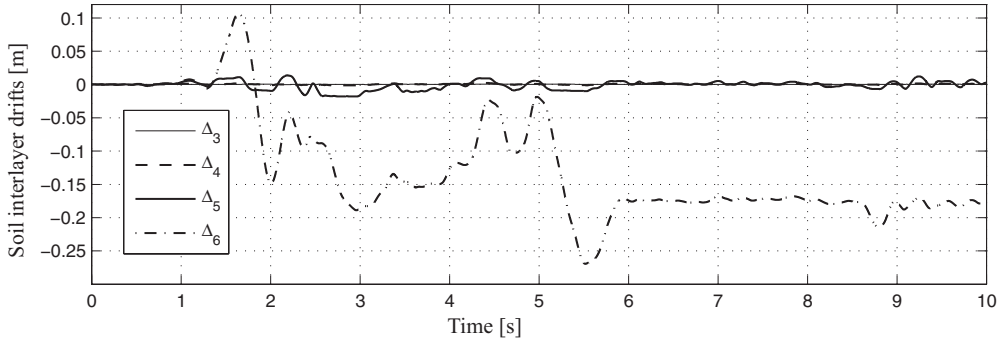

Fig. 5. Response of the 2D SFSI system: time histories of soil interlayer drifts

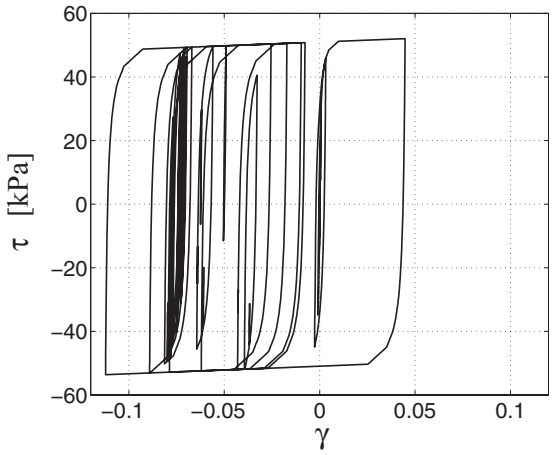

Fig. 7. Response of the 2D SFSI system: shear stress-strain hysteretic response at integration point IP_1 of the soil (see Fig. 1)

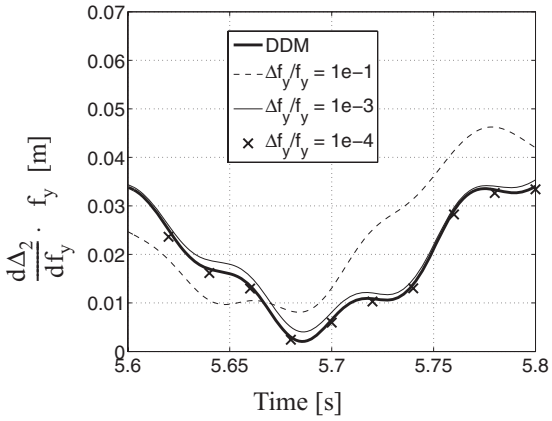

Fig. 9. Validation of DDM results for the 2D SFSI system through FFD analysis: zoom view of normalized sensitivity of first interstory drift to yield stress f_y of reinforcing steel

verified for several global and local response quantities as well as for all sensitivity parameters considered. Due to space limitation, only few of these results are presented here. Fig. 8 shows the asymptotic convergence of FFD-based to DDM-based sensitivities of the first interstory drift (global response quantity) to the yield stress of the reinforcing steel. Fig. 9 provides a zoom view of this convergence trend. Response sensitivities are given in normalized form, i.e., multiplied by the nominal value of the corresponding sensitivity parameter, and can thus be interpreted as one hundred times the change in the response quantity due to one percent change in the sensitivity parameter. These normalized sensitivities directly provide the relative importance of the different parameters on the response quantity of interest. The convergence studies performed validate the analytical formulation and the computer implementation of the DDM algorithms for handling MPCs in regards to the two-dimensional SFSI system considered here as first application example. Fig. 10 displays the time histories of the sensitivities of the frame first interstory drift to the following material parameters: (1) $f_{c,\text{core}}$=strength of core concrete; (2) f_y=yield stress of reinforcing steel; and (3) τ_3=shear strength of the third soil layer (second layer from the bottom). Each of these three parameters, $f_{c,\text{core}}$, f_y, and τ_3, represents the parameter to which the first interstory drift time history is most sensitive for each of the three material types (concrete, reinforcing steel, and soil, respectively). It is noteworthy that, in general, the strength related material parameters become predominant in affecting the system response when the system undergoes significant yielding (Barbato 2007; Gu 2008) as in the present case. As shown in Fig. 10, τ_3 is the parameter with the largest peak absolute value (over the entire time history) of the normalized sensitivities. The sensitivity of Δ_2 with respect to τ_3 remains positive over most of the earthquake duration, indicating that an increase in τ_3 produces an increase in Δ_2. In fact, the value of τ_3 sets a limit on the seismic load that can be transferred from the base of the soil domain to the base of the foundations and therefore to the superstructure. If the earthquake excitation is strong enough to yield the soil, an increase in τ_3 produces larger ground surface acceleration. Fig. 10 also shows that f_y is the second most important parameter in regards to Δ_2. The sensitivity of Δ_2 with respect to f_y is negative over most of the earthquake duration, consistently with the intuitive expectation that an increase in f_y reduces Δ_2, everything else remaining the same.

Three-Dimensional Three-Story Reinforced Concrete Frame Structure with Rigid Diaphragm Behavior at Each Floor

The second application example consists of a three-dimensional, one-bay, three-story reinforced concrete frame building with con-

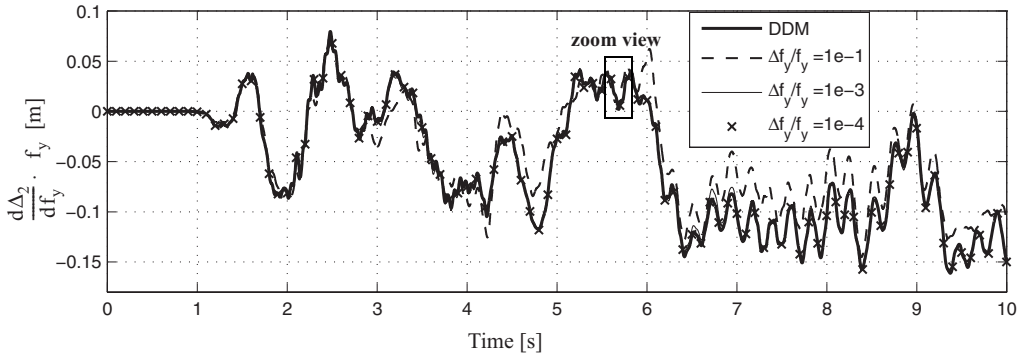

Fig. 8. Validation of DDM results for the 2D SFSI system through FFD analysis: normalized sensitivity of first interstory drift to yield stress f_y of reinforcing steel

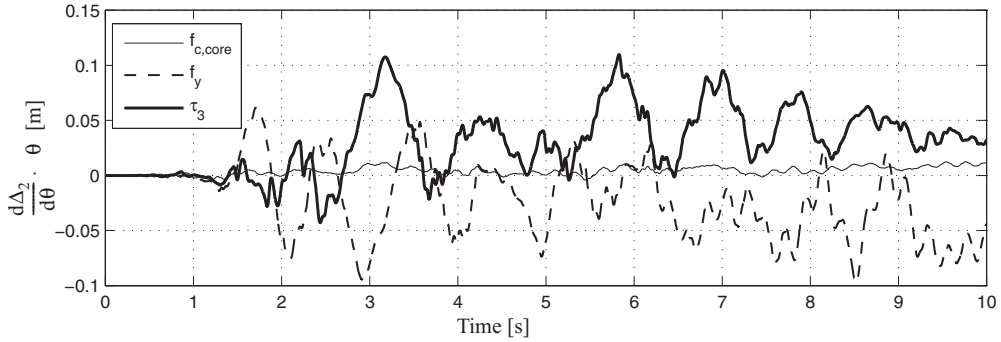

Fig. 10. Response sensitivities of the 2D SFSI system: normalized sensitivities of first interstory drift to most important material parameters

crete slabs at each floor, as shown in Fig. 11. Each story is of height $h=12$ ft ($h=3.66$ m) and the bay is of span $L=20$ ft ($L=6.10$ m) in both horizontal directions. All columns are of squared cross-sectional shape with side $d=18$ in (0.457 m), eight #8 rebars of longitudinal reinforcement and reinforcement cover $c=1.5$ in (0.038 m). All beams have a rectangular cross section 24 in (0.610 m) deep and 18 in (0.457 m) wide.

The floor concrete slabs are modeled through a rigid diaphragm MPC at each floor level. Column and beam members are modeled using two and one, respectively, displacement-based Euler-Bernoulli frame elements with four Gauss-Legendre integration points each. Column cross sections are discretized in fibers of confined concrete, unconfined concrete and steel reinforcement. Beam cross sections are assumed to have a linear elastic behavior. A detailed description of the FE model of this structure is presented elsewhere (Barbato 2007; Gu 2008). The material constitutive models used are (1) the Kent-Scott-Park model for concrete, with parameters $f_{c,\text{core}}=34.5$ MPa, $f_{u,\text{core}}=24.1$ MPa, $\varepsilon_{0,\text{core}}=0.005$, $\varepsilon_{u,\text{core}}=0.020$ for confined concrete, and $f_{c,\text{cover}}=27.6$ MPa, $f_{u,\text{cover}}=0$ MPa, $\varepsilon_{0,\text{cover}}=0.002$, $\varepsilon_{u,\text{cover}}=0.006$ for unconfined concrete, and (2) the one-dimensional J_2 plasticity model for reinforcing steel, with parameters $E=210$ GPa, $f_y=248$ MPa, $H_{\text{kin}}=4.29$ GPa, and $H_{\text{iso}}=0$ Pa.

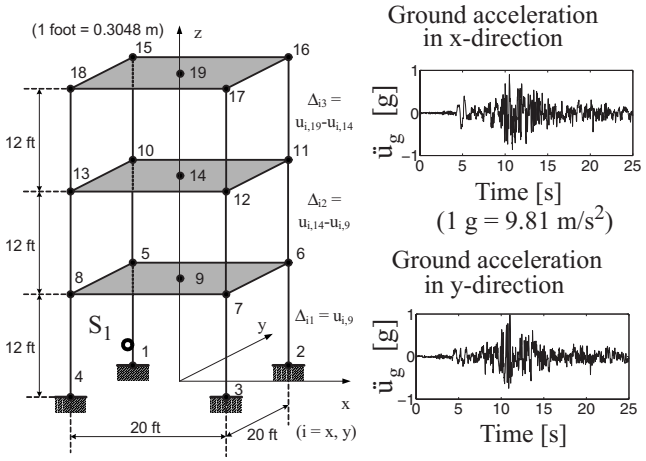

Fig. 11. 3D one-bay three-story reinforced concrete building: structural model and input ground motion

After quasi-static application of the gravity loads, the structure is subjected to a bidirectional earthquake excitation with ground acceleration time histories taken as the two horizontal components of the 1978 Tabas earthquake (see Fig. 11). Figs. 12 and 13 plot the time histories of the interstory drifts in the x- and y-directions, respectively. As expected, the interstory drift is largest for the first story and decreases with story elevation. The peak first interstory drift in the x-direction (0.080 m) is slightly larger than that in the y-direction (0.069 m). These peak interstory drifts correspond to significant interstory drift ratios of 2.20% and 1.89%, respectively. Fig. 14 shows the moment-curvature hysteretic response in the x-direction at the integration point identified as Section 1 (S_1 in Fig. 11). Significant inelastic flexural behavior is observed at this specific location. The irregular ("wavy") moment-curvature hysteresis loops are due to the interaction between axial and bidirectional bending behaviors.

In conjunction with the FE response analysis, a DDM-based response sensitivity analysis is performed, considering as sensi-

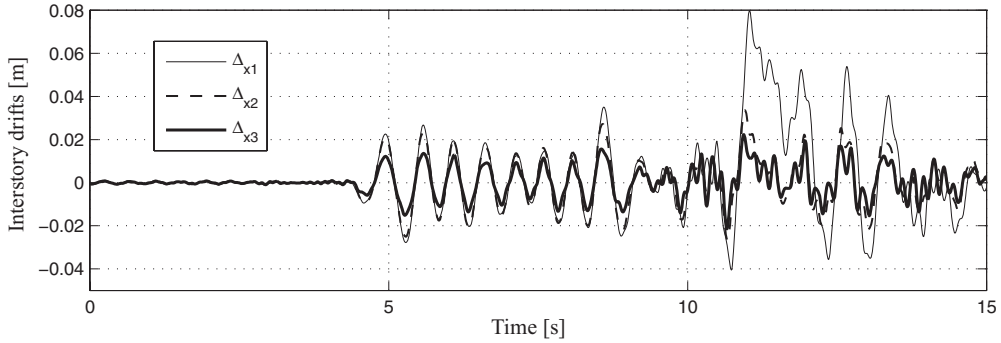

Fig. 12. Response of 3D building: time histories of interstory drifts in the x-direction

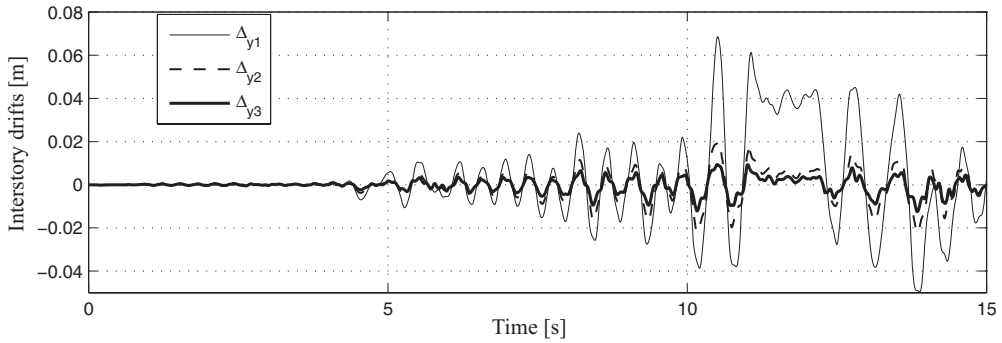

Fig. 13. Response of 3D building: time histories of interstory drifts in the y-direction

tivity parameters the material parameters characterizing the confined concrete (four parameters), unconfined concrete (four parameters), reinforcing steel (four parameters) and the stiffness properties of the elastic beams (one parameter: Young's modulus $E=24.9$ GPa), for a total of 13 material parameters. Fig. 15 shows the asymptotic convergence of FFD-based to DDM-based sensitivities of the first interstory drift (a global response quantity) in the x-direction, considering as sensitivity parameter the compressive strength of the confined concrete f_c. Fig. 16 provides a zoom view of these convergence results. Fig. 17 displays the asymptotic convergence of FFD-based to DDM-based response sensitivity results, in which the moment about the x-axis at Section 1 (a local response quantity) is considered as response quantity and the Young's modulus of the reinforcing steel is considered as sensitivity parameter. A zoom view of the above convergence trend is given in Fig. 18. The results of the convergence studies performed validate the analytical formulation and computer implementation of the DDM algorithms for handling MPCs in the context of this second application example. Fig. 19 plots the sensitivity time histories of the first interstory drift in the x-direction to the Young's modulus of the reinforcing steel E, strength of the unconfined concrete $f_{c,\text{cover}}$, and yield stress of the reinforcing steel f_y. These parameters (in order of decreasing relative importance) are the ones to which the considered response parameter, Δ_{x1}, is most sensitive among all 13 sensitivity parameters considered. In this case, a stiffness related sensitivity parameter (E) is dominant in regards to the first interstory drift Δ_{x1}, suggesting that the plastic deformations experienced by the building frame are limited and the elastic properties control significantly the seismic response behavior of the system.

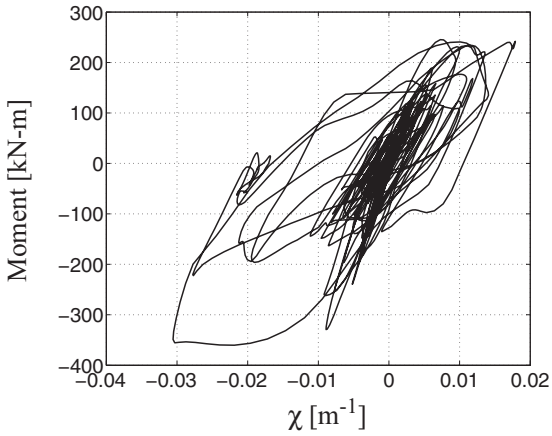

Fig. 14. Response of 3D building: moment-curvature hysteretic response about the x-axis at Section 1 (S_1 in Fig. 11)

Conclusions

This paper presents the extension of the direct differentiation method (DDM) to finite-element (FE) models with multi-point constraints (MPCs). The DDM is an accurate and efficient method for computing FE response sensitivities to material, geometric

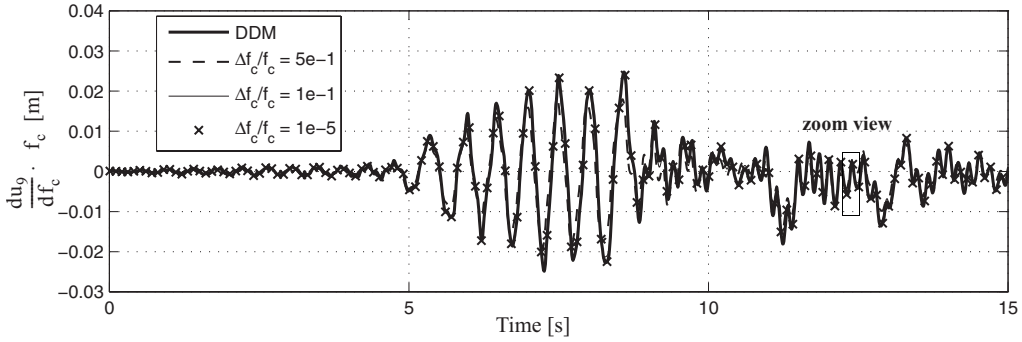

Fig. 15. Validation of DDM results for 3D building through FFD analysis: normalized sensitivity of first interstory drift in the x-direction to core concrete strength f_c

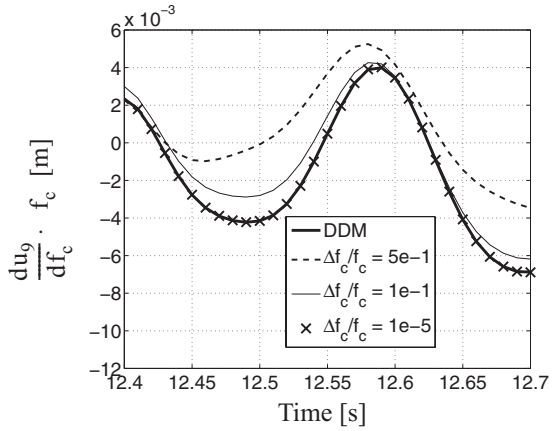

Fig. 16. Validation of DDM results for 3D building through FFD analysis: zoom view of normalized sensitivity of first interstory drift in the x-direction to core concrete strength f_c

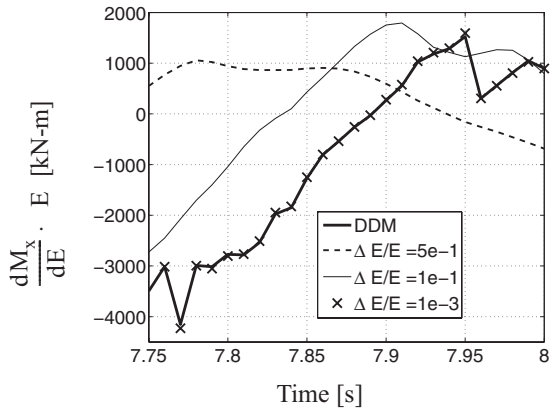

Fig. 18. Validation of DDM results for 3D building through FFD analysis: zoom view of normalized sensitivity of moment response about the x-axis at Section 1 (S_1 in Fig. 11) to Young's modulus E of reinforcing steel

and loading parameters. Response sensitivity algorithms for both quasi-static and dynamic FE analyses are developed for three different constraint handling techniques, namely: (1) the transformation equation method; (2) the Lagrange multiplier method; and (3) the penalty function method.

The response sensitivity algorithms developed in this paper are implemented into a general-purpose nonlinear FE analysis framework. The methodology is illustrated through two application examples: (1) a two-dimensional soil-foundation-structure interaction system subjected to earthquake excitation, and (2) a three-dimensional, one-bay by one-bay, three-story reinforced concrete frame structure with floor slabs modeled as rigid diaphragms subjected to bidirectional earthquake excitation. DDM-based response sensitivities are compared with the corresponding results obtained through forward finite difference (FFD) analyses with decreasing values of the parameter perturbations. Asymptotic convergence of FFD-based to DDM-based response sensitivity results validates the algorithms presented and their computer implementation.

The developments presented in this paper close an important gap between FE response-only analysis and FE response sensitivity analysis through the DDM, extending the latter to applications requiring response sensitivities using FE models with MPCs. Such applications include structural optimization, structural reliability analysis, and finite-element model updating.

Acknowledgments

The writers gratefully acknowledge the support of this research by (1) the National Science Foundation under Grant No. CMS-0010112; (2) the Pacific Earthquake Engineering Research (PEER) Center through the Earthquake Engineering Research Centers Program of the National Science Foundation under Award No. EEC-9701568; and (3) the Louisiana Board of Regents through the Pilot Funding for New Research (Pfund) Program of the National Science Foundation Experimental Program to Stimulate Competitive Research (EPSCoR) under Award No. NSF(2008)-PFUND-86. The writers wish to thank Dr. Frank McKenna for his invaluable help in implementing the response sensitivity algorithms for handling multi-point constraints in OpenSees. Any opinions, findings, conclusions or recommendations expressed in this publication are those of the writers and do not necessarily reflect the views of the sponsors.

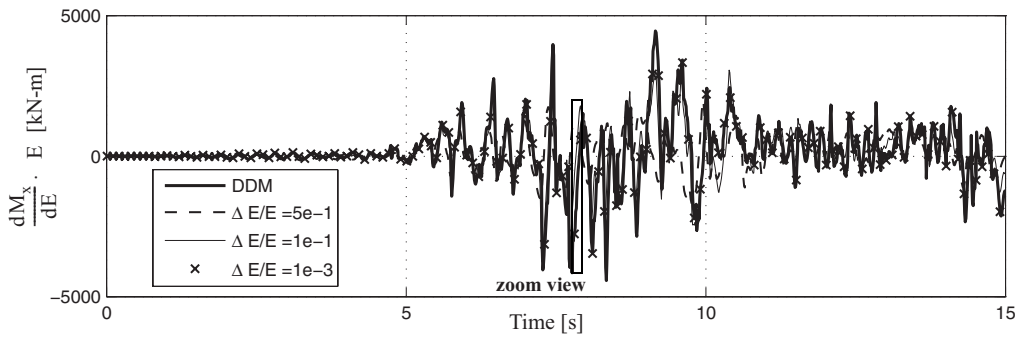

Fig. 17. Validation of DDM results for 3D building through FFD analysis: normalized sensitivity of moment response about the x-axis at Section 1 (S_1 in Fig. 11) to Young's modulus E of reinforcing steel

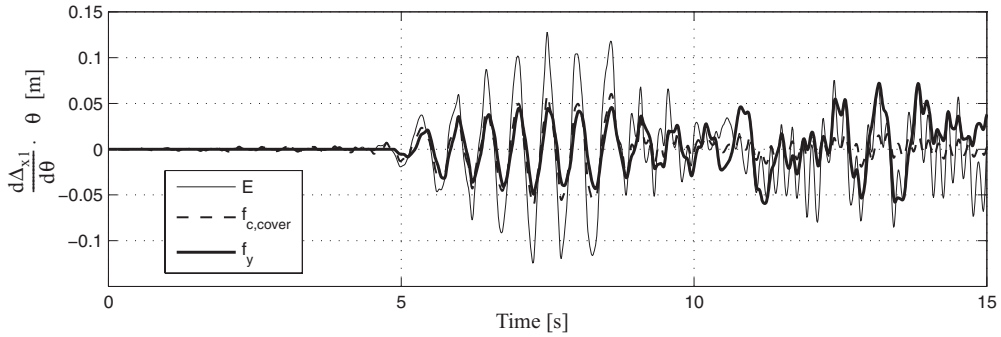

Fig. 19. Response sensitivities of 3D building: normalized sensitivity of first interstory drift in the *x*-direction to most important material parameters

References

Advanced Technology Council (ATC-55). (2005). *Evaluation and improvement of inelastic analysis procedure*, Advanced Technology Council, Redwood City, Calif.

Barbato, M. (2007). "Finite element response sensitivity, probabilistic response and reliability analyses of structural systems with applications to earthquake engineering." Ph.D. dissertation, Dept. of Structural Engineering, Univ., of California at San Diego, La Jolla, Calif.

Barbato M., and Conte J. P. (2005). "Finite element response sensitivity analysis: a comparison between force-based and displacement-based frame element models." *Comput. Methods Appl. Mech. Eng.*, 194(12–16), 1479–1512.

Barbato, M., and Conte, J. P. (2006). "Finite element structural response sensitivity and reliability analyses using smooth versus non-smooth material constitutive models." *Int. J. of Reliability and Safety*, 1(1–2), 3–39.

Barbato, M., Zona, A., and Conte, J. P. (2007). "Finite element response sensitivity analysis using three-field mixed formulation: general theory and application to frame structures." *Int. J. Numer. Methods Eng.*, 69(1), 114–161.

Chopra, A. K. (2001). *Dynamics of structures: Theory and applications to earthquake engineering*, 2nd Ed., Prentice-Hall, Upper Saddle River, N.J.

Conte, J. P. (2001). "Finite element response sensitivity analysis in earthquake engineering." *Earthquake engineering frontiers in the new millennium*, Spencer & Hu, Swets & Zeitlinger, Lisse, The Netherlands, 395–401.

Conte, J. P., Barbato, M., and Spacone, E. (2004). "Finite element response sensitivity analysis using force-based frame models." *Int. J. Numer. Methods Eng.*, 59(13), 1781–1820.

Conte, J. P., Vijalapura, P. K., and Meghella, M. (2003). "Consistent finite element response sensitivity analysis." *J. Eng. Mech.*, 129(12), 1380–1393.

Cook, R. D., Malkus, D. S., Plesha, M. E., and Witt, R. J. (2002). *Concepts and applications of finite element analysis*, 4th Ed., Wiley, New York.

Ditlevsen, O., and Madsen, H. O. (1996). *Structural reliability methods*, Wiley, New York.

Felippa, C. A. (2001). "Introduction to finite element method." Ebook, ⟨http://www.colorado.edu/engineering/CAS/courses.d/IFEM.d/Home.html⟩ (May 10, 2009).

Franchin, P. (2004). "Reliability of uncertain inelastic structures under earthquake excitation." *J. Eng. Mech.*, 130(2), 180–191.

Gu, Q. (2008). "Finite element response sensitivity and reliability analysis of soil-foundation-structure-interaction systems." Ph.D. dissertation, Dept. of Structural Engineering, Univ. of California at San Diego, La Jolla, Calif.

Gu, Q., Conte, J. P., Elgamal, A., and Yang, Z., (2009). "Finite element response sensitivity analysis of multi-yield-surface J_2 plasticity model by direct differentiation method." *Comp. Meth. Appl. Mech. Eng.* 198(30–32), 2272–2285.

Haukaas, T., and Der Kiureghian, A. (2005). "Parameter sensitivity and importance measures in nonlinear finite element reliability analysis." *J. Eng. Mech.*, 131(10), 1013–1026.

Haukaas, T., and Der Kiureghian, A. (2007). "Methods and object-oriented software for FE reliability and sensitivity analysis with application to a bridge structure." *J. Comput. Civ. Eng.*, 21(3), 151–163.

Haukaas, T., and Scott, M. H. (2006). "Shape sensitivities in the reliability analysis of nonlinear frame structures." *Comput. Struc.*, 84(15–16), 964–977.

Kleiber, M., Antunez, H., Hien, T. D., and Kowalczyk, P. (1997). *Parameter sensitivity in nonlinear mechanics: Theory and finite element computations*, Wiley, New York.

Mazzoni, S., McKenna, F., and Fenves, G. L. (2005). "OpenSees Command Language Manual." Pacific Earthquake Engineering Center, University of California, Berkeley, ⟨http://opensees.berkeley.edu/⟩ (May 10, 2009).

Prevost, J. H. (1977). "Mathematical modelling of monotonic and cyclic undrained clay behaviour." *Int. J. Numer. Analyt. Meth. Geomech.*, 1(2), 195–216.

Scott, B. D., Park, P., and Priestley, M. J. N. (1982). "Stress-strain behavior of concrete confined by overlapping hoops at low and high-strain rates." *J. Am. Concr. Inst.*, 79(1), 13–27.

Scott, M. H., and Filippou, F. C. (2007). "Response gradients for nonlinear beam-column elements under large displacements." *J. Struct. Eng.*, 133(2), 155–165.

Scott, M. H., Franchin, P., Fenves, G. L., and Filippou, F. C. (2004). "Response sensitivity for nonlinear beam-column elements." *J. Struct. Eng.*, 130(9), 1281–1288.

Scott, M. H., and Haukaas, T. (2008). "Software framework for parameter updating and finite element response sensitivity analysis." *J. Comput. Civ. Eng.*, 22(5), 281–291.

Zhang, Y., and Der Kiureghian, A. (1993). "Dynamic response sensitivity of inelastic structures." *Comput. Methods Appl. Mech. Eng.*, 108, 23–36.

Zona, A., Barbato, M., and Conte, J. P. (2004). "Finite element response sensitivity analysis of steel-concrete composite structures." *Rep. No. SSRP-04/02*, Dept. of Structural Engineering, Univ. of California, San Diego, Calif.

Zona, A., Barbato, M., and Conte, J. P. (2005). "Finite element response sensitivity analysis of steel-concrete composite beams with deformable shear connection." *J. Eng. Mech.*, 131(11), 1126–1139.

Zona, A., Barbato, M., and Conte, J. P. (2006). "Finite element response sensitivity analysis of continuous steel-concrete composite girders." *Steel Compos. Struct.*, 6(3), 183–202.